◆ Human Brain Mapping 37:2247–2262 (2016) ◆

Investigation of the Electrophysiological Correlates of Negative BOLD Response During Intermittent Photic Stimulation: An EEG-fMRI Study

Eleonora Maggioni,[1,2]* Claudio Zucca,[3] Gianluigi Reni,[4] Sergio Cerutti,[5] Fabio M. Triulzi,[6] Anna M. Bianchi,[5] and Filippo Arrigoni[7]

[1]*Department of Basic Medical Sciences, Neuroscience and Sense Organs, University of Bari 'Aldo Moro', Bari, Italy*
[2]*Department of Neurosciences and Mental Health, Fondazione IRCCS Ca' Granda Ospedale Maggiore Policlinico, University of Milan, Milano, Italy*
[3]*Clinical Neurophysiology Unit, Scientific Institute IRCCS E.Medea, Bosisio Parini, Lecco, Italy*
[4]*Bioengineering Laboratory, Scientific Institute IRCCS E.Medea, Bosisio Parini, Lecco, Italy*
[5]*Department of Electronics, Information and Bioengineering, Politecnico di Milano, Milano, Italy*
[6]*Neuroradiology Unit, Fondazione IRCCS Ca' Granda, Ospedale Maggiore Policlinico, Milano, Italy*
[7]*Neuroradiology Unit, Scientific Institute IRCCS E.Medea, Bosisio Parini, Lecco, Italy*

Abstract: Although the occurrence of concomitant positive BOLD responses (PBRs) and negative BOLD responses (NBRs) to visual stimuli is increasingly investigated in neuroscience, it still lacks a definite explanation. Multimodal imaging represents a powerful tool to study the determinants of negative BOLD responses: the integration of functional Magnetic Resonance Imaging (fMRI) and electroencephalographic (EEG) recordings is especially useful, since it can give information on the neurovascular coupling underlying this complex phenomenon. In the present study, the brain response to intermittent photic stimulation (IPS) was investigated in a group of healthy subjects using simultaneous EEG-fMRI, with the main objective to study the electrophysiological mechanisms associated with the intense NBRs elicited by IPS in extra-striate visual cortex. The EEG analysis showed that IPS induced a desynchronization of the basal rhythm, followed by the instauration of a novel rhythm driven by the visual stimulation. The most interesting results emerged from the EEG-informed fMRI analysis, which suggested a relationship between the neuronal rhythms at 10 and 12 Hz and the BOLD dynamics in extra-striate visual cortex. These findings support the hypothesis that NBRs to visual stimuli may be neuronal in origin rather than reflecting pure vascular phenomena. *Hum Brain Mapp 37:2247–2262, 2016.* © 2016 Wiley Periodicals, Inc.

Key words: EEG-fMRI; negative BOLD; visual stimulation

Additional Supporting Information may be found in the online version of this article.

Contract grant sponsor: Fondazione Cariplo (project #2010-0344, "Spider@Lecco"); Contract grant sponsor: European Union's Seventh Framework Programme for research, technological development and demonstration; Contract grant number: 602450

*Correspondence to: Eleonora Maggioni, Bioengineering Laboratory, Scientific Institute IRCCS E. Medea, via Don Luigi Monza 20, 23842, Bosisio Parini, Lecco, Italy. E-mail: emaggioni@bp.lnf.it or eleonora.maggioni@polimi.it

Received for publication 20 April 2015; Revised 19 February 2016; Accepted 22 February 2016.

DOI: 10.1002/hbm.23170
Published online 14 March 2016 in Wiley Online Library (wileyonlinelibrary.com).

INTRODUCTION

Functional Magnetic Resonance Imaging (fMRI) based on blood oxygenation level dependent (BOLD) contrast is a powerful technique providing a measure of cortical and subcortical brain function with high spatial resolution. Despite its high sensitivity and specificity, fMRI has the drawback to be sensitive to the hemodynamic/metabolic processes in the brain, which are only indirectly related to neuronal activity [Logothetis and Wandell, 2004; Logothetis et al., 2001].

As a consequence, the interpretation of fMRI findings in terms of the underlying neuronal processes is not always straightforward. The majority of fMRI studies focuses on brain regions with positive BOLD responses, which are thought to reflect evoked neuronal activity [e.g., Boorman et al., 2010; Logothetis et al., 2001]. Nonetheless, increasing interest is being received by regions with a negative BOLD response, whose underlying mechanisms are still largely unknown.

In recent years, different multimodal approaches have been adopted to obtain a more complete view of the phenomenon of negative BOLD, but its origin and properties are still debated [Bressler et al., 2007; Huber et al., 2014; Müller and Kleinschmidt, 2004; Mullinger et al., 2014; Shmuel et al., 2002; Smith et al., 2004; Wade, 2002]. Two main competitive theories explain the negative BOLD in terms of either "vascular stealing" or "neuronal suppression," but the most recent evidences support the neuronal hypothesis over the vascular one [Bressler et al., 2007; Mullinger et al., 2014; Smith et al., 2004; Wade, 2002]. In support of the theory of neuronal inhibition is a recent multimodal study, which found that NBRs in sensorimotor cortex corresponded to reduction in (1) cerebral blood flow (CBF), (2) mu power and (3) somatosensory evoked potentials [Mullinger et al., 2014].

Recently, Near Infrared Spectroscopy (NIRS) has been used with fMRI to investigate the intense negative BOLD responses elicited by intermittent photic stimulation in healthy subjects [Maggioni et al., 2013, 2015]. The fMRI study revealed a complex pattern of response during IPS, in which the expected positive BOLD response (PBR) in primary visual cortex was accompanied by a negative BOLD response (NBR) in two symmetric regions in Lateral Occipital Cortex (LOC). In turn, the NIRS study allowed to investigate the vascular aspects of NBRs: it confirmed the presence of a negative hemodynamic response (i.e., inverted compared to the canonical one) to IPS in LOC and showed that NBRs corresponded to an increase of deoxy-hemoglobin (HHb) concentration accompanied by a higher decrease of oxy-hemoglobin (HbO) concentration. The combination of NIRS and fMRI contributed to increase the knowledge of negative BOLD, but left open questions on the origin of the oxygenation changes highlighted by the two techniques. The neuronal activity associated with negative BOLD in visual cortex can be investigated through electroencephalography (EEG), which measures the synchronized electrical activity of large populations of neurons with high temporal resolution.

In the present study, simultaneous EEG-fMRI data were acquired from a group of 21 healthy volunteers during an IPS protocol, with the primary objective to study the neurovascular coupling underlying the NBRs to IPS. To extract extensive information on the effects of IPS in visual cortex, we performed both unimodal and multimodal analysis of EEG-fMRI data. The fMRI response to IPS was first investigated with a General Linear Model (GLM) activation analysis, followed by spatial and temporal analysis of the regions significantly involved. Then, the EEG information was used to study the time-varying frequency content in the occipital channels. The complementary information were finally integrated in an EEG-informed fMRI analysis, with the objective to investigate the hemodynamic correlates of the EEG power changes in the IPS frequencies.

MATERIALS AND METHODS

Subjects

A group formed by 21 healthy volunteers (9 males, mean age 27.6 ± 2.15 years) took part to the study. All of them had normal vision and negative history for epileptic seizures or any other neurological or vascular disease.

The experimental procedure was approved by the Institutional Ethic Committee and was carried out in accordance with the Declaration of Helsinki. Each volunteer signed a written consent after adequate information about the scope and methodology of the study.

Experimental Protocol

The visual stimulation protocol was developed using the Presentation® software (Neurobehavioral Systems). The protocol, already described in [Maggioni et al., 2013, 2015] proved to be effective in evoking both PBR and NBR in visual cortex. It consisted of blocks of IPS alternated with blocks of resting state, each lasting seven fMRI scans (corresponding to 14 s). The IPS was created by reversing black and white screens at four frequencies, 6, 8, 10 and 12 Hz, which were presented in progressive order. Each frequency block was repeated five times, resulting in twenty IPS blocks. The subjects kept their eyes open during the entire experiment, while during resting phases they gazed upon a yellow cross in the center of the black screen. The total duration of the fMRI exam was 594 s, including 7 initial and 10 final dummy scans.

MRI Data Acquisition

The MRI acquisition was performed on a 3T scanner (Philips Achieva, Best, The Netherlands), equipped with a 32-channels head coil. The fMRI data were acquired with a T2*-weighted Gradient-Echo planar sequence (repetition

time (TR) = 2 s, echo time (TE) = 35 ms, flip angle = 85°, 30 axial slices without gap, field of view (FOV) = 240 × 240 × 105 mm^3, voxel size = 1.875 × 1.875 × 3.5 mm^3) covering cerebral hemispheres, excluding cerebellum and brainstem. A structural MR image was acquired with a T1-weighted 3D Turbo Field Echo sequence (1 mm isotropic resolution, FOV = 240 × 240 × 175 mm^3, TR = 8.19 ms, TE = 3.74 ms, flip angle = 8°) to provide a morphological reference for fMRI data. Visual stimuli were delivered in the MR scanner through MR-compatible goggles (Resonance Technology Inc.).

EEG Data Acquisition

EEG data were recorded simultaneously with fMRI recordings using an MR-compatible EEG system (BrainAmp MR plus from Brain Products, Gilching, Germany). The EEG cap (BrainCap MR, EasyCap GmbH, Breitbrunn, Germany) included 63 scalp electrodes distributed according to the 10–20 system and one additional electrocardiographic (ECG) electrode placed on the participants' chest. All EEG signals were relative to a reference located in FCz, with the ground in correspondence of AFz. The EEG data were sampled at 5,000 Hz by applying a band-pass filtering of 0.016–250 Hz. The impedance at each electrode was kept lower than 20 kΩ.

fMRI Data Processing

The processing of fMRI data was performed in Matlab 8.3.0.532 (R2014a) using toolboxes and in-house scripts.

Preprocessing

The fMRI data of each subject were processed with the Statistical Parametric Mapping (SPM) software (http://www.fil.ion.ucl.ac.uk/spm/, version 8) [Penny et al., 2011]. The preprocessing included spatial realignment for reducing head motion artifacts, coregistration of the structural image to the mean functional image, normalization to the MNI template and spatial smoothing with a 3D Gaussian kernel filter with Full Half Width Maximum (FHWM) of 6 mm. The spatial normalization parameters were estimated from the structural image and applied to all functional images.

Activation analysis with GLM and ROI analysis

The IPS blocks were convolved with the canonical Hemodynamic Response Function (HRF) [Penny et al., 2011] and used as regressor of interest in a GLM. The six movement parameters were added as confounding regressors. The effects of IPS compared to rest condition were first assessed at the single-subject level by making inference with a two sided *t*-test. The contrast images (IPS > rest) resulting from the first level analysis of the subjects were used in a second level random-effects analysis, which allowed to account for the intersubject variability and make inference at the population level [Beckmann et al., 2003]. The information about the significant regions resulting from the group analysis (*t*-contrast: IPS > rest and IPS < rest, significance: $P < 0.05$, peak-Family Wise Error (pFWE) and cluster-False Discovery Rate (cFDR) corrected) were saved with the SPM Marsbar toolbox (http://marsbar.sourceforge.net/) [Brett et al., 2002], which is a tool that provides features for ROI analysis. The anatomical position of the ROIs was determined by coregistration with the subcortical and cortical Harvard-Oxford atlas (http://www.cma.mgh.harvard.edu) [Desikan et al., 2006]. The GMAC toolbox (http://selene.bioing.polimi.it/BBBlab/GMAC) [Tana et al., 2012] was used to extract from all subjects the BOLD time series (already subjected to the above preprocessing) corresponding the each significant ROI (contrast: IPS > rest, IPS < rest, $P < 0.05$, pFWE corrected and cFDR corrected). The BOLD signals were extracted after removal of the nuisance variables, that is, the remaining sources of spurious variance [Tana et al., 2012]. The representative BOLD signal of each ROI was calculated by averaging the BOLD time series of the voxels within the ROI. The BOLD responses to IPS in these ROIs were inspected from frequency to frequency and their temporal and amplitude parameters were calculated. A Kruskal Wallis (KW) analysis was performed considering each parameter in the ROIs and across subjects to reveal possible significant differences. When significant differences were detected among all the ROIs, post-hoc pairwise comparisons were performed; *P*-values lower than 0.01 were considered as significant.

A further GLM activation analysis was performed to study the response to the single IPS frequencies (contrasts: 6 Hz/8 Hz/10 Hz/12 Hz >/< rest). The regions activated by IPS at the single IPS frequencies were highly overlapped, indicating a uniform effect of IPS from 6 to 12 Hz, therefore the results will not be shown.

EEG Data Processing

The EEG data preprocessing was performed with BrainVision Analyzer 2.0 software (BrainProducts, Gilching, Germany). First, the gradient artifact (GA) was removed from the data by subtracting from each channel a template created using a sliding average of 21 blocks of the artifact. The cleaned EEG and ECG signals were downsampled to 250 Hz and subjected to a low pass filter with cut-off frequency of 70 Hz. A semi-automatic procedure allowed to mark the R peaks on the ECG signal, which were used to correct the pulse artifact (PA). For this purpose, the Average Artifact Subtraction method (AAS) [Allen et al., 2000] was applied: the intervals of occurrence of the artifact were used to construct a PA template for each channel, which was then removed from each artifact. To correct the residual cardiac related artifact, together with other noise related to ocular and generic movements, we applied an extended Infomax ICA [Lee et al., 1999]. The ICA mixing

matrix was computed from the whole data by discarding the bad intervals, that is, those affected by substantial artifacts, which were manually marked by the user. The independent components (ICs) were segmented into PA intervals (from 0 to 700 ms with respect to the R peaks) and those related to the PA were identified using the selection method based on their continuous wavelets transform (CWT) presented in [Maggioni et al., 2014]. The selection of the artifactual ICs was also based on a careful visual inspection of the IC time series. This combined approach allowed to mark the ICs with even a small PA contribution, while preserving the ones that exhibited IPS-related changes. The EEG signal reconstructed from the nonartifactual ICs was checked for the presence of residual bad intervals. The corrected EEG data were exported to Matlab and used for the following analyses, based on in-house scripts.

To check for the possibility to recover the physiological EEG response to IPS from EEG-fMRI data, we compared the results obtained from EEG data recorded during IPS (1) at 0T and (2) at 3T in one exemplar subject. The results (not shown in the manuscript) show that the main effects of IPS can be satisfactorily recovered also from EEG data recorded simultaneously to fMRI data, after correction of the EEG artifacts with proper algorithms.

The EEG analysis was conducted as follows. We investigated the time-frequency content of the EEG responses to IPS by computing the CWT in epochs going from 6 s before to 6 s after the onset of each IPS block. The CWT was calculated using the Morlet wavelet family (central frequency = 0.813 Hz) defined in the frequency range 1–20 Hz with 0.2 Hz steps. In this analysis, we focused on the occipital channels, O1, O2 and Oz, corresponding to the recipient zone of the photic stimulation; the three channels were considered separately.

The results were first evaluated through visual inspection of (1) the 2D CWT and (2) the 1D plot of the CWT time course in the IPS frequencies. Specifically, for each IPS frequency, the CWTs of O1, O2 and Oz were averaged over IPS epochs (excluding the ones with bad intervals) and subjects.

We then performed quantitative analyses on the effects induced by IPS, considering each subject and occipital channel separately. To study the frequency shifts induced by IPS, we extracted from the CWT the main EEG frequency in each time sample: the EEG frequency was then averaged during rest, using from 2 to 6 s before IPS onset and during IPS at each frequency, using from 2 to 6 s after the IPS onset. A paired *t*-test was then used to compare the EEG frequency from rest to IPS across the 21 subjects.

To provide a quantitative measure of the change of power from rest to IPS, we extracted the EEG power at 6, 8, 10 and 12 Hz during (1) rest, (2) IPS at the same frequency and (3) IPS in general. For each occipital channel, the former was compared with the others: specifically, a paired *t*-test was performed to extract any significant EEG power changes elicited by IPS at the group level. The ratio between the mean power during IPS (in the first 6 s) and rest (in the last 6 s) was used as index for IPS-induced changes. In the above comparisons, a multiple comparison correction was applied using the Bonferroni criterion: specifically, the threshold *P*-value was divided for the number of tests, 12, equal to the number of occipital channels (3) multiplied by the number of frequencies (4). For the sake of completeness, both uncorrected and corrected results will be shown; the reported *P*-values are uncorrected, unless otherwise specified.

To investigate the effects of IPS offsets, the same CWT analysis was performed on epochs going from 6 s before to 6 s after the offset of each IPS block. In this case, the results were just qualitatively evaluated through visual inspection of the 2D CWT.

EEG-fMRI Integration: BOLD Correlates to EEG Rhythms at the IPS Frequencies

The information about the time varying frequency components of the EEG signal was used to investigate the BOLD response to changes in the neuro-electrical oscillatory activity during IPS. For each subject of the group, the CWT was computed on the entire EEG signal using the above parameters. Following the approach of [Laufs et al., 2003; Sclocco et al., 2014], we considered only the channels that were most involved in the neuronal response to IPS, in our study the occipital channels. In particular, we averaged the CWTs of O1, O2 and Oz. The time varying power of the EEG signal at each IPS frequency was estimated as the squared module of the CWT in the frequency of interest. To avoid possible artifactual contributions, the bad EEG intervals were replaced with the mean EEG value across the first 20 s of acquisition, provided that no artifacts occurred in that timespan.

In preparation for the EEG-informed fMRI analysis, the four signals representing the time varying power at 6, 8, 10 and 12 Hz IPS were convolved with the canonical HRF [Penny et al., 2011] and downsampled to match the frequency sampling of the fMRI scans (fs= 0.50 Hz). For each subject, the resulting time series were used as regressors of interest in a first level GLM analysis, where they were fitted to the subject's fMRI data. A fixed-effects GLM analysis was performed, in which the design matrix included the regressors of all subjects. In both the analyses, inference was based on positive and negative *t*-tests that inspected the effects of the time varying EEG power at each IPS frequency.

Since the choice of the GLM parameters can significantly influence the results, we checked whether the assumption of canonical HRF was reliable by conducting a further GLM analysis using as basis set the canonical HRF and its derivatives. The group results of the two analyses were comparable, which let us assume that the form of the hemodynamic response in our subjects generally

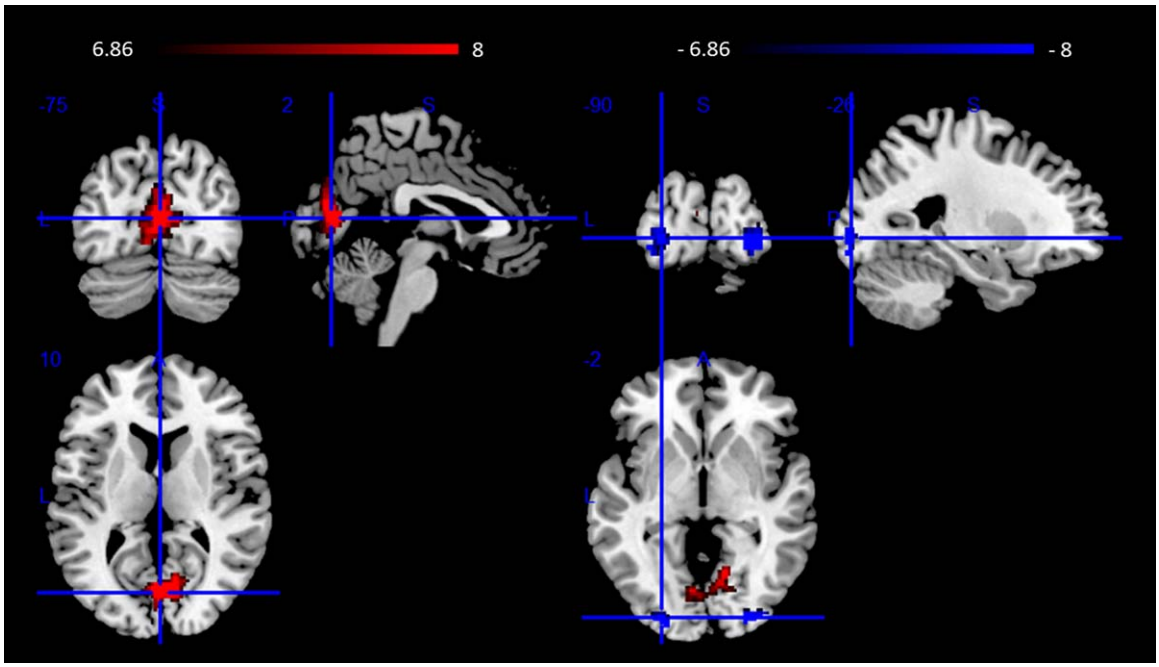

Figure 1.
Results of fMRI GLM group analysis on IPS effects. The significant regions of positive (red) and negative (blue) BOLD response to IPS are overlaid on a normalized canonical image (ch2better template) using the MRIcron software (http://www.mccauslandcenter.sc.edu/mricro/mricron/). ($P < 0.05$, pFWE corrected and cFDR corrected). [Color figure can be viewed in the online issue, which is available at wileyonlinelibrary.com.]

resembled the canonical HRF. Therefore, we will show the results relative to the GLM based on the canonical HRF.

The regions showing a significant response to the four EEG regressors in the fixed-effects group analysis ($P < 0.05$, cluster-FWE (cFWE) corrected), either negative or positive, were saved and the relative time series were extracted in all subjects, following the procedure described in paragraph "Activation analysis with GLM and ROI analysis." In each subject, we quantitatively compared the temporal trend of each EEG regressor with the average signal of each ROI through a correlation analysis. For each ROI, the significance of the correlation coefficient across subjects was evaluated using a one-sample *t*-test. The results will be briefly reported.

RESULTS

GLM fMRI Analysis

The results of the second level fMRI GLM analysis are displayed in Figure 1, where the regions with significant response to IPS that emerged from the double-sided *t*-test ($P < 0.05$, pFWE corrected and cFDR corrected) are overlaid on a normalized canonical image. The red and blue colors indicate regions with positive and negative response to IPS, respectively.

These results confirm and add statistical significance to the fMRI findings of [Maggioni et al., 2013, 2015], which were based on a smaller group. A large region of PBR to IPS was identified in primary visual cortex, on the mesial surface of the occipital lobes. Two symmetric regions characterized by NBR to IPS were detected in extra-striate visual cortex of both hemispheres. Since these regions resulted from a random effects analysis, both PBR and NBRs were highly reproducible across subjects and significant.

The position and extension of the significant ROIs ($P < 0.05$, pFWE corrected and cFDR corrected) are listed in Table I. The PBR area included lingual gyrus, intracalcarine cortex, supracalcarine cortex, cuneal cortex and occipital pole of both hemispheres, while the NBR areas were located in the inferior division of lateral occipital cortex, occipital fusiform gyrus and occipital pole.

The temporal trends of the PBR and NBR to IPS at the group level (relative to the ROIs of Table I) are displayed in Figure 2 and their quantitative parameters are listed in Table II. The two negative responses closely resemble each other, as confirmed by the absence of significant differences in the time and amplitude parameters revealed by the pairwise comparisons, but exhibited some differences with respect to PBR. Despite the PBR and NBR times of peak were similar, the ascent of the NBRs was delayed with respect to the PBR. Major differences were found in the

TABLE I. Coordinates of centre of mass (in MNI space), volume and anatomical position (Harvard-Oxford atlas) of the significant ROIs of the fMRI analysis ($P < 0.05$, pFWE corrected and cFDR corrected) L: left hemisphere. R: right hemisphere

Contrast	Centre of mass (mm)	Volume (mm^3)	HO regions
IPS PBR	4.68 −74.5 11.3	10,416	calcarine cortex, cuneus and lingual gyrus, L, R
IPS NBR1	31.3 −89 −4	1,582	lateral inferior occipital cortex and occipital pole, R
IPS NBR2	−27.1 −91.1 −4.79	1,176	lateral inferior occipital cortex and occipital pole, L

L: left hemisphere. R: right hemisphere.

onset times (i.e., when the signal goes beyond the 5% of the maximum amplitude) and falling edges (i.e., when the signal drops down the 50% of the maximum after the end of the IPS blocks), as the KW statistics revealed significant differences in both of them ($P < 0.01$). Indeed, the NBR onset was significantly delayed compared to PBR, while the NBR falling edge occurred significantly earlier than the PBR one ($P < 0.01$), due to the higher slope of the descent.

Considering the BOLD responses to the single IPS frequencies in the ROIs of Table I, no significant differences emerged from one frequency to another in any of the parameters (peak amplitude and time, onset time and falling edge). The parameters are not reported in the manuscript.

EEG Wavelets Analysis

The group CWT of the EEG responses to IPS in the three occipital channels are displayed in Figure 3, for each IPS frequency separately. The most evident effect of IPS was the immediate desynchronization of the basal alpha rhythm, replaced after around 1 s by a novel EEG rhythm with higher power and with a main frequency that was still in the alpha band but appeared lightly shifted compared to the basal one. This behavior, common to all the three occipital channels, was more noticeable in the lateral ones, which exhibited a higher EEG power increase compared to Oz, and in response to IPS at 8, 10 and 12 Hz. With the exception of IPS at 10 Hz, which centered the basal alpha rhythm to the stimulation frequency, no apparent photic driving was induced by IPS at 6, 8 and 12 Hz.

The results of the quantitative analysis on the main EEG frequency are in agreement with the above observations. During resting state, on average across the occipital channels, the main EEG rhythm was centered at 9.78 Hz (± 0.44 Hz). IPS at 6 Hz brought the alpha peak to a mean value of 10.06 Hz (± 0.55 Hz). Such a frequency increase resulted significant from the paired *t*-test in O1 ($P < 0.05$, Bonferroni corrected) and O2 ($P < 0.01$, Bonferroni corrected). The effects of 8 Hz stimulation were nonsignificant and more heterogeneous in the group: on average, the main EEG frequency during IPS at 8 Hz was 9.9 Hz (± 0.75 Hz). As expected, the 10 Hz IPS did not change significantly the main EEG frequency, bringing it to a mean value of 9.92 Hz (± 0.53 Hz). On the contrary, we found that IPS at 12 Hz induced a significant increase of the main EEG frequency in all the occipital channels ($P < 10^{-4}$, Bonferroni corrected), bringing it to 10.24 Hz (± 0.49 Hz). Still, the EEG rhythm was not moved to the stimulation frequency, thus confirming the findings emerged from visual inspection of the CWT.

The power changes in the four IPS frequencies from resting state to IPS at the same frequency are plotted in Figure 4. Whichever was the IPS frequency, the IPS caused an initial desynchronization of the basal rhythm that lasted up to 2 s. The left and right dynamics were generally synchronized and symmetric. The level of synchronization of the rhythm to the IPS frequency varied from frequency to frequency. By observing the plots, it emerges that IPS at 6 and 8 Hz did not elicit a clear increase in EEG power at the frequency of stimulation, whereas IPS at 10 and 12 Hz provoked a gain of power in the EEG rhythm at the IPS frequency. The biggest increase of power from rest to IPS in the stimulation frequency was caused by IPS at 12 Hz.

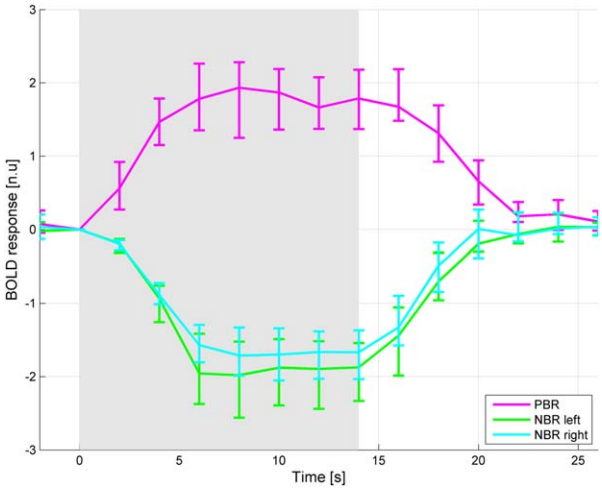

Figure 2.
BOLD response to IPS in the significant ROIs at the group level ($P < 0.05$, pFWE corrected and cFDR corrected, Table I). The main curve is the median, whereas the error bars indicate the 25 and 75 percentiles of the subjects' mean responses. The BOLD responses are in normalized units: they were extracted with SPM8 after "Global normalization" with the default option "session-specific grand mean scaling." The grey background represents the stimulation period. [Color figure can be viewed in the online issue, which is available at wileyonlinelibrary.com.]

TABLE II. Quantitative parameters of the ROIs with PBR and NBR to IPS (Table I; 25, 50 and 75 percentiles from subject to subject, where the mean response of each subject is considered)

	Peak time (s)			Peak amplitude (n.u.)			Onset time (s)			Falling edge (s)		
	25%	50%	75%	25%	50%	75%	25%	50%	75%	25%	50%	75%
PBR	6	8	10	1.47	1.94	2.41	0.25	0.33	0.55	18.15	18.95	20.15
NBR L	6	8	10	1.62	2.13	2.64	0.62	0.92	1.45	16.38	17.01	17.47
NBR R	6	8	10	1.56	1.71	2.17	0.59	0.9	1.28	16.45	16.72	17.72

L: left hemisphere. R: right hemisphere.

These qualitative findings were confirmed by the results of the quantitative analyses: the ratios of EEG power at 6, 8, 10 and 12 Hz from rest to IPS at the corresponding frequency (mean and standard deviation across subjects) are listed in Table III, upper part. The significant power changes are marked with * ($P < 0.05$), ** ($P < 0.01$) and *** ($P < 0.05$, Bonferroni corrected). IPS at 6 Hz was found to induce a significant increase of 6 Hz power in the Oz channel ($P < 0.05$), but not in O1 and O2. This finding can be confirmed by looking at the 2D CWT of Figure 3, showing the instauration of the 6 Hz rhythm in the mesial occipital area. The EEG power at 8 and 10 Hz did not change significantly after IPS at the corresponding frequencies, whereas IPS at 12 Hz elicited a significant power increase at 12 Hz in all occipital channels ($P < 0.01$), overcoming the multiple comparison correction in O1 ($P < 0.05$, Bonferroni

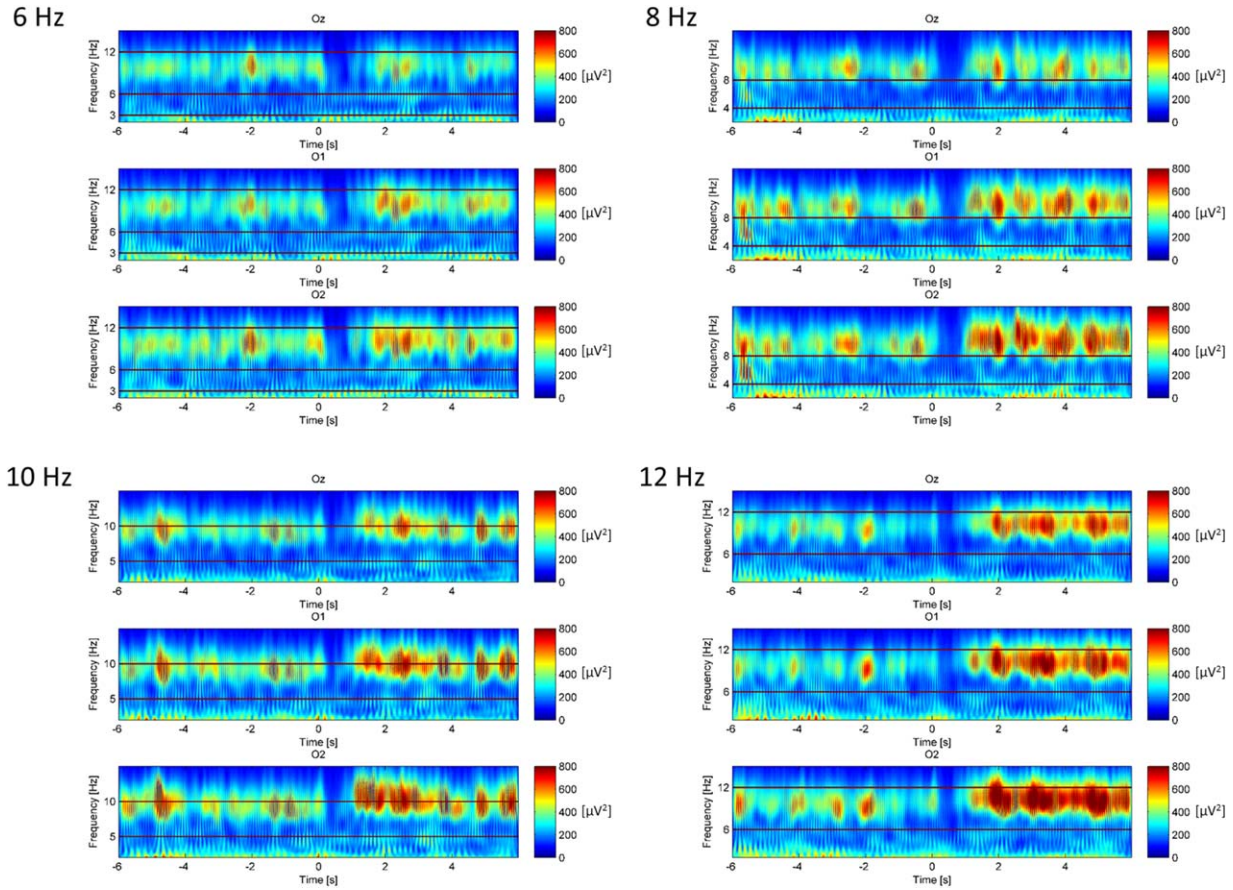

Figure 3.

CWT of the EEG signal averaged over subjects, in the IPS intervals going from −6 s to +6 s with respect to IPS onset, at 6, 8, 10 and 12 Hz, in Oz, O1 and O2 channels (from first to third row of each panel). The red lines indicate the IPS frequency and its harmonics. [Color figure can be viewed in the online issue, which is available at wileyonlinelibrary.com.]

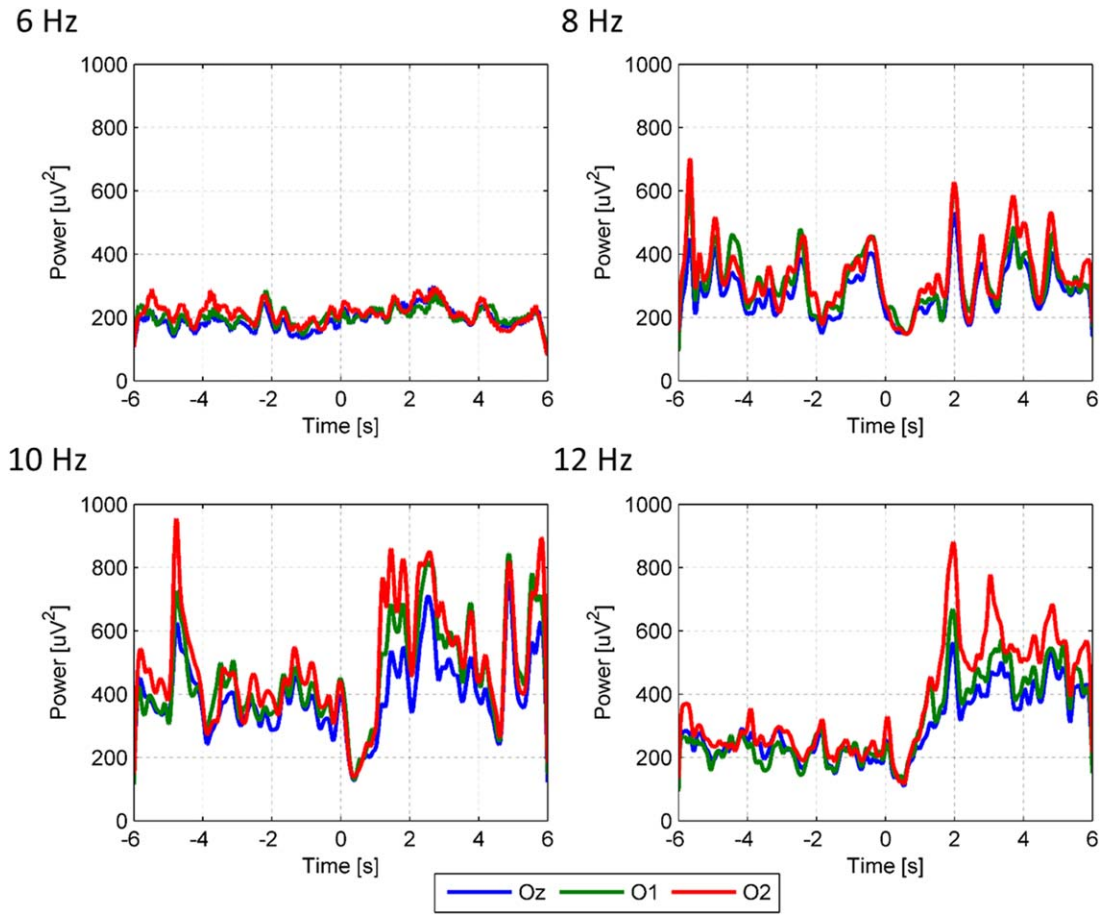

Figure 4.

Plot of the CWT in the first IPS harmonic averaged over subjects, in the IPS intervals going from −6 s to +6 s with respect to IPS onset, relative to IPS at 6, 8, 10 and 12 Hz, in Oz, O1 and O2 channels. [Color figure can be viewed in the online issue, which is available at wileyonlinelibrary.com.]

corrected). This power increase was more enhanced in the lateral occipital channels compared to the central ones.

Looking at the power changes at 6, 8, 10 and 12 Hz from rest to IPS in general, that is, at all frequencies, similar findings emerged (Table III, lower part). A significant increase of 8 Hz power was induced by IPS in the left occipital channel, O1 ($P < 0.05$). The 10 Hz EEG power significantly increased from resting state to IPS in both O1 ($P < 0.01$) and O2

TABLE III. Ratios between EEG power at 6, 8, 10 and 12 Hz during IPS and during rest, for IPS in the same frequency (upper rows) and IPS at all frequencies (lower rows)

		EEG Power ratio (IPS/rest)		
		Oz	O1	O2
IPS in the same frequency	6 Hz	1,16 ± 0,27*	1,08 ± 0,39	1,01 ± 0,26
	8 Hz	1,36 ± 0,84	1,17 ± 0,44	1,17 ± 0,40
	10 Hz	1,90 ± 1,28	1,69 ± 0,83	1,67 ± 0,83
	12 Hz	1,79 ± 0,73**	1,92 ± 0,81***	1,97 ± 0,85**
IPS at all frequencies	6 Hz	1,06 ± 0,21	0,99 ± 0,16	1,00 ± 0,15
	8 Hz	1,20 ± 0,45	1,14 ± 0,22*	1,11 ± 0,23
	10 Hz	1,52 ± 0,75	1,55 ± 0,66**	1,55 ± 0,71*
	12 Hz	1,55 ± 0,69*	1,63 ± 0,69***	1,71 ± 0,87*

The significant power changes are marked with * ($P < 0.05$), ** ($P < 0.01$) and *** ($P < 0.05$, Bonferroni corr).

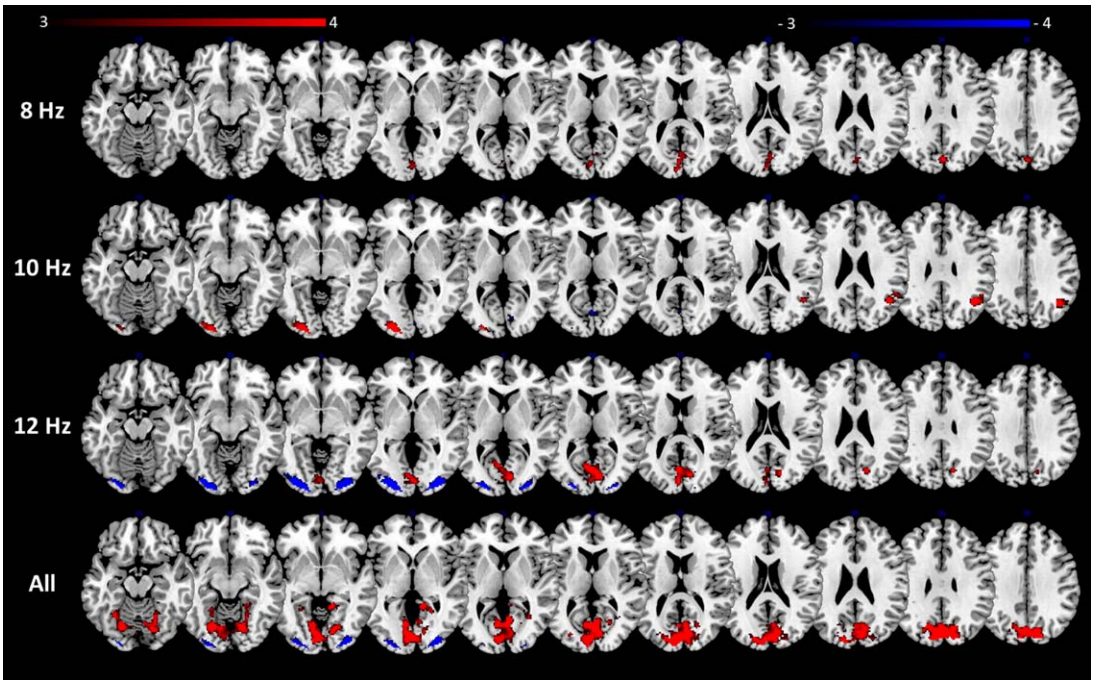

Figure 5.

Regions with significant BOLD response ($P < 0.05$, cFWE corrected) to EEG power changes at 8, 10 and 12 Hz and at all IPS frequencies. Blue regions are relative to negative BOLD responses, red regions to positive BOLD responses. The ROIs are overlaid on a normalized canonical image (ch2better template) using the MRIcron software (http://www.mccauslandcenter.sc.edu/mricro/mricron/). [Color figure can be viewed in the online issue, which is available at wileyonlinelibrary.com.]

($P < 0.05$). A significant increase of 12 Hz EEG power from rest to IPS was detected in all occipital channels, Oz ($P < 0.05$), O1 ($P < 0.05$, Bonferroni corrected) and O2 ($P < 0.05$).

The effects of the IPS offset on the brain electrical activity are displayed in the Supporting Information Figure 1. As expected, the cessation of the photic stimulation provoked an abrupt desynchronization of the neuronal activity in all the occipital channels. The EEG rhythm that was driven by the photic stimulation was again replaced after 1–2 s by the resting state EEG activity, which showed a main frequency peak in the alpha band and was characterized by an overall lower EEG power compared to IPS EEG activity. The results demonstrate that the EEG response to IPS was sustained across the entire block of stimulation, being continuously characterized by increased EEG power compared to the baseline condition.

The patterns of light-on and light-off EEG power decrease were similar, except from the fact that, while the decrease in alpha power due to IPS onset occurred within the first 200 ms of IPS, the end of the IPS-induced synchronization was delayed of 250–500 ms with respect to IPS offset.

EEG-fMRI Integration

The regions with significant response to the EEG power changes at 6, 8, 10 and 12 Hz, considered both separately and in conjunction, ($P < 0.05$, cFWE corrected) are shown in Figure 5, whereas their position and extension are listed in Table IV.

No significant ROIs from the 6 Hz contrasts survived the multiple comparison correction, whereas a region in primary visual cortex spanning the two hemispheres, located in calcarine cortex and cuneus, responded positively to the 8 Hz EEG power changes.

A portion of the bilateral calcarine cortex showed BOLD dynamics that were in counterphase with respect to the 10 Hz EEG changes, whereas two regions in left inferior occipital cortex and in right angular gyrus showed a positive BOLD response to the 10 Hz EEG dynamics. Similar positive BOLD responses emerged also in the corresponding portions of the opposite hemispheres, but these regions did not survive to the FWE correction.

Regarding the 12 Hz contrast, a big region in primary visual cortex responded positively to the rise of 12 Hz EEG power, which was clearly associated with the IPS onset. Instead, two symmetric regions in lateral occipital cortex were negatively correlated with the 12 Hz EEG rhythm. The portions of inferior occipital cortex with PBR to EEG dynamics at 10 Hz and NBR to EEG dynamics at 12 Hz already emerged in the fMRI analysis for having a NBR to IPS.

The regions with significant BOLD response to all the EEG regressors are visible in the lower panel of Figure 5.

TABLE IV. Coordinates of centre of mass (in MNI space), volume and anatomical position (Harvard-Oxford atlas) of the significant ROIs of the EEG-informed fMRI analysis ($P < 0.05$, cFWE corrected) L: left hemisphere. R: right hemisphere

Contrast	Centre of mass (mm)	volume (mm^3)	HO regions
8 Hz PBR	−0.35 −80.2 17.2	4,004	cuneus and calcarine cortex, L, R
10 Hz PBR1	−24.9 −90.5 −4.48	3,262	inferior occipital cortex and occipital pole, L
10 Hz PBR2	44.8 −57.6 29.3	3,262	angular gyrus and superior lateral occipital cortex R
10 Hz NBR	2.06 −76.3 9.45	910	calcarine cortex, L, R
12 Hz PBR	1.37 −76.5 10.6	9,212	calcarine cortex, cuneus and lingual gyrus, L, R
12 Hz NBR1	−27.6 −88.5 −3.8	4,998	Lateral inferior occipital cortex and occipital pole, L
12 Hz NBR2	29.2 −88.6 −1.51	3,780	Lateral inferior occipital cortex and occipital pole, R
All frequencies PBR	0.67 −74 9.1	42,112	calcarine cortex, cuneus and lingual gyrus, L, R
All frequencies NBR1	−26.6 −91.4 −5.01	1,638	Lateral inferior occipital cortex and occipital pole, L
All frequencies NBR2	29.4 −89.4 −1.69	1,638	Lateral inferior occipital cortex and occipital pole, R

On average, we found a PBR in the primary visual cortex, specifically in bilateral calcarine cortex, cuneus and lingual gyrus and a NBR in the bilateral inferior occipital cortex.

To help understand the link between the results of the fMRI and EEG-informed fMRI analyses, we have extracted the mean BOLD response to IPS from the ROIs with significant BOLD response to the EEG regressors (Table IV). Figure 6 shows the group BOLD responses to IPS blocks at 8, 10, 12 Hz and all frequencies in the significant ROIs responding to the EEG power changes at the considered frequency/frequencies. The results show that almost all these regions responded to IPS. The bilateral inferior occipital regions with significant NBR to the 12 Hz EEG power changes also exhibited a negative response to IPS blocks at 12 Hz. Similarly, a negative BOLD response to IPS at 10 Hz was detected in the portion of left inferior occipital cortex with significant PBR to the 10 Hz EEG regressor, which was included in the 12 Hz ROI. Conversely, the regions in primary visual cortex with positive response to the EEG power changes at 8 and 12 Hz, as well as the ones with negative response at 10 Hz, responded positively to IPS at the corresponding frequency. The ROI in right angular gyrus was an exception, as it responded positively to the 10 Hz EEG rhythm but did not show any significant response to IPS.

Figure 7 shows, for one exemplar subject, the BOLD fluctuations in the significant ROIs of the 8, 10 and 12 Hz EEG contrasts together with the corresponding EEG regressors. In each subplot, relative to one EEG contrast, the intervals corresponding to IPS blocks at the frequency of interest are colored in grey. In this subject, the EEG regressors, especially the 8 and 12 Hz ones, provided a good fit of the BOLD responses in the significant ROIs. The reverse temporal trend of the inferior occipital ROIs with respect to the 12 Hz regressor is particularly evident, as well as the positive correlation between the 8 and 12 Hz EEG dynamics and the BOLD ones in primary visual cortex.

From the correlation analysis between EEG regressors and BOLD time series in the significant ROIs (Table IV), performed from subject to subject, we found the presence at the group level of (1) a significant positive correlation ($P < 0.01$) between the ROI in left lateral inferior occipital cortex with the corresponding 10 Hz regressor, (2) a significant negative correlation between the symmetric ROIs in lateral occipital cortex and the 12 Hz regressor.

These results suggest that the NBRs to IPS may be positively and negatively associated with the variations of EEG power at 10 and 12 Hz respectively, possibly reflecting the changes from the basal rhythm to a novel "driven" rhythm during IPS. These hypotheses are discussed in detail in the next paragraph.

DISCUSSION

In the present work, the physiological response to IPS was investigated from multiple perspectives, looking at neuronal and hemodynamic mechanisms and at their interaction. Simultaneous EEG-fMRI data were recorded from a group of 21 healthy volunteers during IPS at four frequencies, from 6 to 12 Hz. The analysis of data from each modality was followed by an integrated analysis, which investigated the BOLD correlates to variations of EEG power in the four IPS frequencies.

Our main objective was the investigation of the electrophysiological phenomena underlying the complex fMRI activation pattern induced by IPS, characterized by both positive and negative BOLD responses in striate and extrastriate portions of visual cortex.

While PBRs are commonly interpreted as activations, the origin of NBRs represents a matter of discussion in the literature [e.g., Goense et al., 2012; Huber et al., 2014; Mullinger et al., 2014; Shmuel et al., 2006]. There are a number of previous studies that reported concomitant PBR and NBR to different visual stimuli [Bressler et al., 2007; Goense et al., 2012; Huber et al., 2014; Shmuel et al., 2002; Smith et al., 2000; Tootell et al., 1998]; however, in our study the NBRs to IPS were found to be more intense, with a peak amplitude comparable to the PBR one and occupied a bigger area compared to previously emerged NBRs.

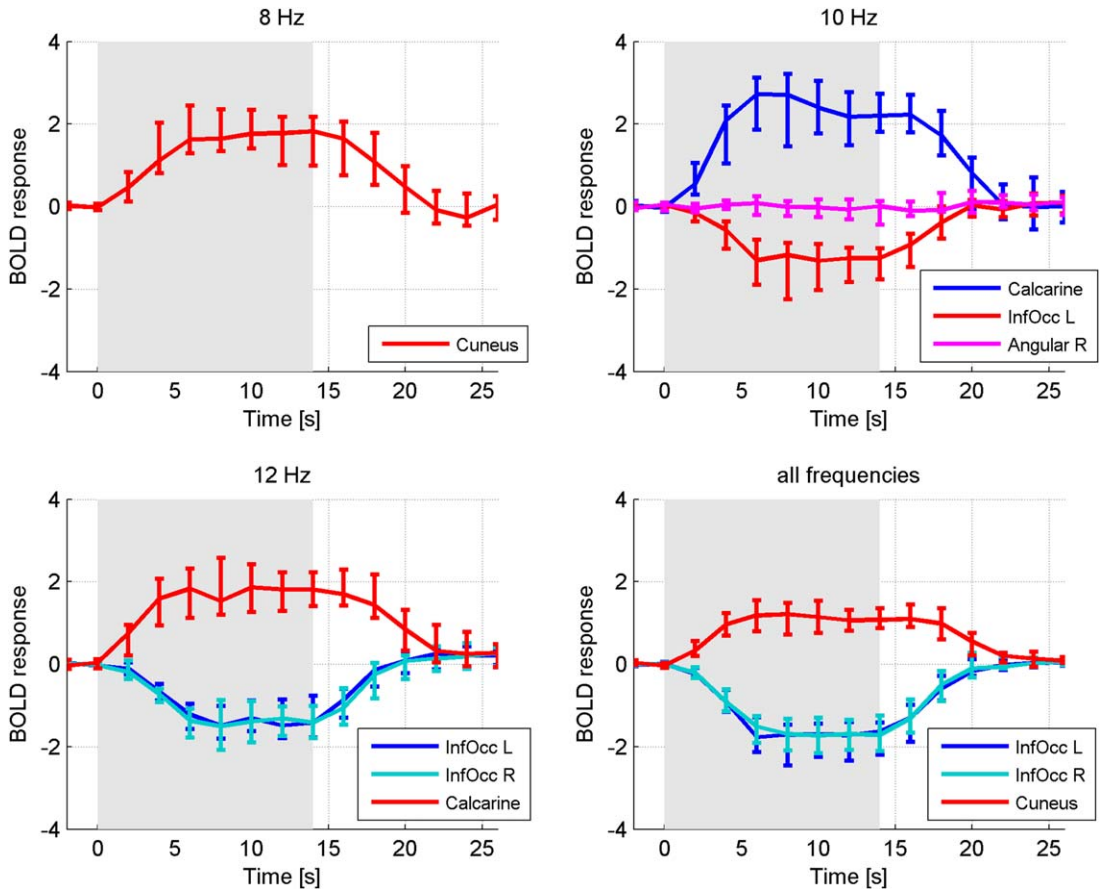

Figure 6.

Group BOLD response to IPS blocks at 8, 10, 12 Hz and at all frequencies in the ROIs with significant BOLD response to the EEG power changes at the corresponding frequency/frequencies (Table IV). The grey background represents the stimulation period. The main curve is the median, whereas the error bars indicate the 25 and 75 percentiles of the subjects' mean responses. The BOLD responses are in normalized units: they were extracted with SPM8 after "Global normalization" with the default option "session-specific grand mean scaling." [Color figure can be viewed in the online issue, which is available at wileyonlinelibrary.com.]

In [Maggioni et al., 2015], the vascular properties of NBRs to IPS were investigated through an optical technique, NIRS, able to differentiate between HbO and HHb contributions. In the lateral portion of occipital cortex, where the NBRs were located, the two hemoglobin species had an inverted response to IPS with respect to the canonical one. The estimated total hemoglobin (THb) changes suggested that NBRs may correspond to a decrease in cerebral blood volume (CBV), that is, a vasoconstriction. The findings of this previous study were consistent with the hypothesis that NBRs correspond to decreases of both CBF and $CMRO_2$ and are neuronal in origin [e.g., Mullinger et al., 2014]. Nonetheless, the neuronal hypothesis was not supported by direct knowledge of neuronal activity during IPS.

With the present EEG-fMRI study, we have provided information on the neuronal response to IPS and shed light onto the coupling between neuronal and hemodynamic activities. Furthermore, we have added statistical evidence to the previous fMRI findings, which were based on a smaller sample. To our knowledge, the present work is the first to explore (1) the neuronal response to IPS in subjects keeping eyes open, (2) the BOLD responses to EEG power changes induced by photic stimulation in healthy subjects and (3) the electrophysiological mechanisms underlying negative BOLD in visual cortex.

Furthermore, the findings of the present study can be used as reference for future studies on photosensitivity. Indeed, a full comprehension of the physiological mechanisms associated to IPS is an essential preliminary step towards the in-depth analysis of pathological modifications underlying photoparoxysmal responses (PPR). In the literature, there are a number of IPS studies conducted on patients keeping their eyes closed [Bjørk et al., 2011; Lazarev et al., 2015; Visani et al., 2010]; the effects of IPS on

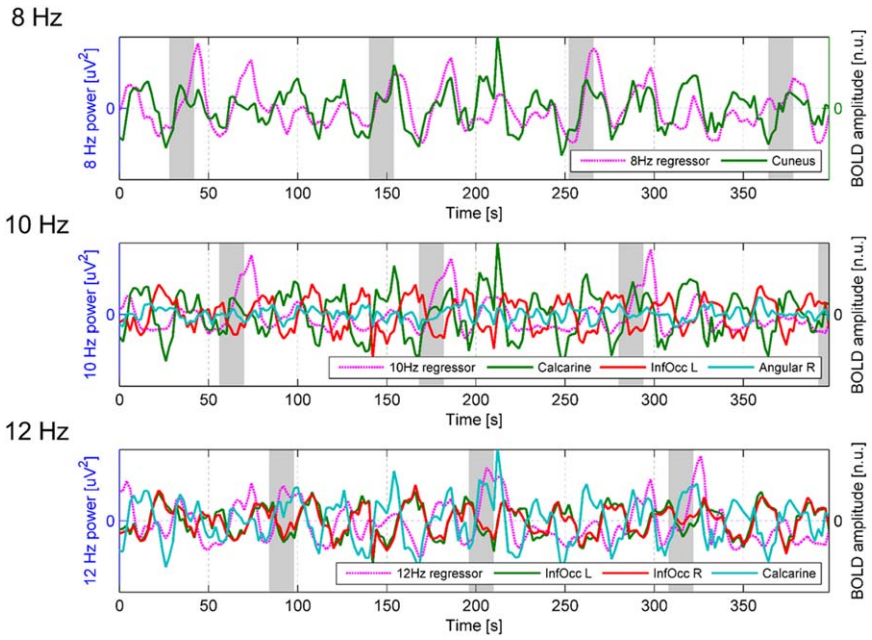

Figure 7.

BOLD dynamics in the significant ROIs of the 8, 10 and 12 Hz EEG contrasts (Table IV) together with the corresponding EEG regressors. The dynamics are plotted during the first 200 s of IPS protocol. The grey bars indicate IPS blocks at the corresponding frequency. The BOLD responses are in normalized units: they were extracted with SPM8 after "Global normalization" with the default option "session-specific grand mean scaling." [Color figure can be viewed in the online issue, which is available at wileyonlinelibrary.com.]

subjects with eyes open that are described here can be used as normative to understand photosensitive phenomena elicited by stimuli in the daily environment, which occur when the subjects are awake.

Neuronal Response to IPS

The time-frequency analysis of EEG data revealed that IPS caused, in the occipital channels, a desynchronization of the basal EEG rhythm, lasting 1–2 s, followed by a novel rhythm driven by the visual stimulation.

Normal subjects may exhibit a physiological "photic driving" response to IPS, which is characterized by a rhythmic EEG activity at the frequency of stimulation or one of its harmonics and is visible mainly in the occipital region [Visani et al., 2010]. The results of our study suggest that, in subjects keeping their eyes open, the photic stimulation is usually unable to move the basal EEG rhythm to the stimulation frequency, unless the latter is near the resting state frequency. On average, we found that the EEG rhythm induced by IPS was still in the alpha band and was characterized by higher EEG power. Only the stimulation at 12 Hz elicited a significant frequency shift towards the IPS frequency.

The alpha power decrease that occurred immediately after the IPS onset is a consistent and reproducible phenomenon that was already observed in a previous study conducted on subjects with eyes closed [Kawabata, 1972], which has been defined as "photic alpha blocking." After the blocking, the instauration of a new EEG rhythm characterized by higher EEG power suggests that the photic stimulation enhances the neuronal oscillatory synchronization. The IPS offset induced a desynchronization of the stimulation rhythm and an EEG power decrease, followed by the restauration of the resting state EEG activity.

The absence of a clear harmonic synchronization to the IPS frequency may be due to the fact that the subjects kept their eyes open during all the experiment.

However, at the group level, IPS induced an increase of EEG spectral power at the frequency of stimulation. The most interesting evidence concerns the 12 Hz EEG rhythm, which exhibited a power increase in all occipital channels during IPS at 12 Hz but also, on average, during IPS at all frequencies, thus suggesting a key role of this rhythm during our IPS experiment. In the left occipital area, such an increase was significant even after Bonferroni correction. The enhanced power differences at 12 Hz may be related to the fact that the 12 Hz rhythm was not present at baseline but fully elicited by the photic stimulation.

IPS in general was found to induce an EEG power increase at 8 and 10 Hz, result that is in agreement with the observation of increased alpha power during IPS.

Similarly to IPS at 12 Hz, we found that this increase was enhanced in the left occipital area than in the right one, supporting the physiological photic driving laterality that was reported in previous studies [Hirota et al., 2001; Lansing and Thomas, 1964].

Although the interpretation of these EEG findings is not straightforward, they represent relevant pieces of information that can help the interpretation of the complex fMRI activation pattern during IPS.

EEG-fMRI Integration During Photic Stimulation

The EEG-informed fMRI analysis provided additional information on the physiological processes underlying IPS: not surprisingly, we found a relationship between the EEG power changes at the IPS frequencies and the fMRI activations in visual cortex.

In response to the four EEG regressors, we found a large PBR in primary visual cortex and two symmetric NBRs in lateral occipital cortex. The fact that these anatomical regions correspond to the ROIs with significant response to IPS in the fMRI analysis supports the reliability of our results.

For what concerns the single EEG regressors, it emerged that no regions at the group level responded significantly to the EEG power changes at 6 Hz. On the light of the modest 6 Hz power fluctuations detected in the EEG analysis, this results was somehow expected. Accordingly, the activation in primary visual cortex related to the 8 and 12 Hz power changes may be linked to the photic stimulation. However, the biggest PBR in primary visual cortex was found in response to EEG rhythm at 12 Hz, which was the frequency exhibiting the most significant increase of EEG power from rest to IPS.

On the contrary, the inverse relationship that emerged between the 10 Hz EEG dynamics and the BOLD signal in primary visual cortex may be due to the fact that the baseline rhythm was centered approximately at 10 Hz. Therefore, although IPS induced an increase of the 10 Hz power, the 10 Hz EEG power changes were also representative of the resting state dynamics. The activation of lateral occipital cortex and angular gyrus in response to the 10 Hz EEG rhythm may be interpreted accordingly: indeed, (1) the former region showed a negative BOLD response to IPS, (2) the angular gyrus has been shown to be a key node of the Default Mode Network (DMN) [Greicius et al., 2003] thus supporting the hypothesis of the 10 Hz rhythm as resting state rhythm.

Very informative results emerged also from the 12 Hz negative contrast: indeed, a negative correlation was detected between the 12 Hz EEG power changes and the BOLD response in bilateral occipital cortex. This region exhibited a negative response to IPS and included the area with positive response to the 10 Hz EEG rhythm. It is worth remarking that the BOLD dynamics in the lateral occipital regions were found to be significantly correlated with the 10 and 12 Hz regressors across subjects, thus demonstrating a high interindividual reproducibility of these results.

These findings suggest a link between the NBRs to IPS and the EEG dynamics at 10 and 12 Hz and support the hypothesis that NBRs to IPS are neuronal in origin. On the one hand, the positive correlation between the 10 Hz EEG rhythm and the BOLD fluctuations in inferior occipital regions may indicate an involvement of these regions in the resting state condition. Such hypothesis is borne out by literature evidence, which shows the presence of an extra-striate visual network among the resting state networks [Beckmann et al., 2005; van den Heuvel and Pol, 2010].

Alternatively, NBRs to IPS may be related to the significant increase of 12 Hz EEG power elicited by IPS, which occurred on average across all IPS frequencies, as revealed by the EEG time-frequency analysis. The coupling between NBRs to IPS and 12 Hz rhythm may also explain the time differences between positive and negative BOLD responses to IPS. Indeed, the delayed onset of the NBRs may be related to the delayed increase in 12 Hz power, which followed the initial desynchronization of the baseline rhythm and therefore was shifted in time of 1–2 s with respect to the IPS onset.

Although their interpretation is extremely delicate, these important evidences confirm the added value of the integration of EEG and fMRI information, which facilitates the difficult interpretation of the results coming from the single modalities. This analysis has allowed to confirm the relationship between neuronal activity and negative BOLD, which was only hypothesized in several studies on negative BOLD [e.g., Bressler et al., 2007; Wade, 2002]. However, future investigations are needed to determine the mechanisms underlying the possible coupling between the 10 and 12 Hz rhythms and NBRs to IPS.

It is worth mentioning that Moosman et al. [2003] reported an inverse relation between spontaneous alpha EEG oscillations and BOLD signal in occipital cortex. However, the occipital region that emerged from their study included both striate and extra-striate visual cortex. Moreover, in our study the EEG power changes reflected the alternation of resting state and stimulation instead of spontaneous variations during resting state, which makes the comparison of the results more difficult. When discussing their results, Moosman et al. suggested that neuronal synchronization might either require less energy or be associated with reduced input from other neuronal sources. In our study, IPS increased the neuronal synchronization in the alpha band but induced both "activations" and "deactivations" in visual cortex, thus complicating the interpretation of our findings.

Neurovascular Coupling Underlying Positive and Negative BOLD Responses

The fMRI information depends on a series of vascular parameters that represent only surrogates for the

underlying neuronal activity. In this respect, there are still unanswered questions concerning the relationship of BOLD variations with actual neural activation.

Logothetis and colleagues demonstrated that a spatially localized BOLD increase directly and monotonically reflects an increase in neuronal activity. They also suggested the BOLD signal to be more related to local field potentials (LFPs), reflecting the incoming input and local processing of one brain region, rather than to spiking activity itself [Logothetis et al., 2001]. Since the BOLD effect is a composite function of CBF, CBV and $CMRO_2$, important efforts have been done to understand the mutual relation among these three mechanisms and in turn their link with neuronal activity. Recent evidence explains BOLD in terms of two independent and parallel responses, the hemodynamic and metabolic ones, which are possibly driven by different aspects of neuronal activity [Buxton, 2012]. While $CMRO_2$ is thought to reflect the energy expenses of neuronal activity, CBF seems to be related to neuronal signaling processes through the glutamatergic and cholinergic systems [Murta et al., 2015]. Although the neurophysiology, hemodynamic and metabolism underlying positive BOLD response have been largely unveiled, less is known on the mechanisms responsible for negative BOLD responses.

In the last decades, the origin of NBRs has been explained either in terms of "vascular stealing," that is, that NBRs result from pressure-related blood flow changes during a certain task, or in terms of neuronal inhibition. The most recent studies on negative BOLD have come to the conclusion that NBRs should reflect a reduction in neuronal activity rather than pure vascular mechanisms [Bressler et al., 2007; Mullinger et al., 2014; Smith et al., 2004; Wade, 2002]. This theory is also in line with the hypotheses of decreased CBF and $CMRO_2$ and vasoconstriction, which were put forward in [Maggioni et al., 2015; Mullinger et al., 2014; Shmuel et al., 2002].

Nonetheless, the theory of neuronal inhibition has been originally formed on the basis of CBF, CBV and $CMRO_2$ measurements or estimations [Bressler et al., 2007; Smith et al., 2004; Wade, 2002]. Using concurrent 2D optical imaging spectroscopy and electrophysiology, Boorman et al. [2010] hypothesized that NBRs to whisker stimulation originate from reduced multi-unit activity in deep cortical layers, but without directly measuring the BOLD response. Only recently, Mullinger and colleagues provided direct evidence that NBRs in sensorimotor cortex are neuronal in origin, at least in part [Mullinger et al., 2014].

In our study, for the first time, we investigated the NBRs to visual stimuli by means of the EEG technique, providing a further proof of an actual relationship between neuronal activity and negative BOLD responses. It is worth noticing that no evidence of neuronal inhibition comes from our findings, as we just detected a linear coupling between 10 and 12 Hz rhythms in the occipital channels and BOLD fluctuations in the two NBR regions of the fMRI study. Since the EEG power changes in the three occipital channels were similar, we considered a global measure of neuronal activity in the occipital cortex. Such a similarity was certainly influenced by the volume conduction effects affecting the EEG recordings [van den Broek et al., 1998], which prevented from measuring local neuronal activity in the NBR areas.

Despite the above limitation, our results suggest that negative BOLD may not reflect an actual neuronal inhibition. This hypothesis is in line with findings of [Devor et al., 2005], which showed an antagonistic center-sorround spatial pattern of fMRI response in rodent somatosensory cortex, where the negative response did not correspond to local neuronal inhibition. According to this and our study, the neurovascular transfer function may be nonlocal.

Methodological Limitations

Simultaneous EEG-fMRI recordings represent the most promising noninvasive technique for the study of neurovascular coupling. Nevertheless, there are a number of limitations of both the single modalities and their integration that have to be considered.

As just mentioned, the fMRI acquisitions based on the BOLD contrast provide a complex information of brain metabolism and hemodynamics, which can make the interpretation of fMRI activation patterns challenging. Moreover, despite the good spatial resolution of the fMRI technique, the slow dynamics characterizing BOLD changes and the low fMRI sampling rate cause the ill-posed temporal problem, as it is hard to extract the timings of events that caused the measured hemodynamic modifications [Logothetis, 2008].

Conversely, the EEG technique provides a direct measure of electric potentials with an excellent temporal resolution, but at larger scale compared to other (invasive) electrophysiological techniques. The electrophysiological signals recorded on the scalp can be explained by infinite configurations of neuronal sources. Consequently, the reconstruction of EEG current sources from the scalp recordings represent an ill-posed problem with no unique solution [Grech et al., 2008; Murta et al., 2015; Pascual-Marqui et al., 2002]. More local measures of electrophysiological activity are provided by invasive modalities like intracranial EEG (icEEG), which however cannot be recommended if it is not necessary.

The simultaneity of EEG and fMRI recordings is known to provide important advantages compared to separate acquisitions, but also implies a suboptimal data quality, which in turn may affect the reliability of the EEG-informed fMRI analyses. Indeed, instrumental interactions lead to data contamination and sophisticated correction methods have to be applied in order to recover the underlying physiological information; the mechanisms of EEG

data degradation are largely discussed in [Maggioni et al., 2014], where a set of methods for cleaning the cardiac-related artifact is presented. It has to be specified that in the present work we have used the method for PA removal that resulted most effective in [Maggioni et al., 2014], and the good quality of EEG signals after preprocessing was verified by visual inspection. Moreover, by comparing the EEG responses to IPS at 0T and at 3T we proved that the main effects of IPS can be satisfactorily recovered also from EEG data recorded in the MR environment. Although the limitations of the EEG and fMRI techniques add uncertainty to the interpretation of EEG-fMRI results, the integration of these techniques still represents the best approach to investigate, in a noninvasive way, the neurovascular coupling. The results of our study show the importance of combining EEG and fMRI information in the investigation of the determinants of negative BOLD. A better knowledge of neurovascular coupling can be obtained using MR scanners with higher field strength and EEG caps with high-density electrodes. At ultra-high field, the enhanced spatial resolution of fMRI combined with the excellent temporal resolution of EEG open up the horizon for a detailed assessment of neurovascular coupling at the columnar and laminar level [Neuner et al., 2013]. Moreover, a robust neuronal source reconstruction using a high-density EEG cap may allow to estimate the neuronal activity at a spatial resolution comparable to fMRI one.

In the near future, we are also interested in integrating the EEG and fMRI information using alternative approaches. For instance, the use of fMRI activation patterns as priors in the EEG source reconstruction (fMRI-informed EEG analysis) may help localize the regions of neuronal activation and inhibition. A symmetric EEG-fMRI fusion may be performed by applying a joint Independent Component Analysis (joint-ICA) [Moosman et al., 2008], which offers the possibility to assess the neuronal and hemodynamic information in a common data space.

CONCLUSION

In the present article, a set of methods for the unimodal and multimodal analysis of EEG and fMRI data was used to give insight into the brain response to photic stimulation in a group of healthy subjects. Our primary aim was to study the neuronal underpinnings of NBRs to IPS, which occurred in extra-striate visual cortex in concomitance to the expected PBR in primary visual cortex. The EEG-informed fMRI analysis unveiled a relationship between NBRs to IPS and the 10 and 12 Hz EEG rhythms, thus suggesting a neuronal origin of the negative BOLD phenomenon. Although this hypothesis is in agreement with the most recent literature on negative BOLD, our findings leave many questions on the ratio behind this relationship, which have to be addressed in the next future.

ACKNOWLEDGMENTS

The authors wish to thank Elena Vassena for her precious contribution to the EEG-fMRI acquisitions. The data were acquired during the PhD of EM, which was performed in the Scientific Institute IRCCS E. Medea and in Politecnico di Milano.

REFERENCES

Allen PJ, Josephs O, Turner R (2000): A method for removing imaging artifact from continuous EEG recorded during functional MRI. Neuroimage 12:230–239.

Beckmann CF, Jenkinson M, Smith SM (2003): General multilevel linear modeling for group analysis in FMRI. Neuroimage 20: 1052–1063.

Beckmann CF, DeLuca M, Devlin JT, Smith SM (2005): Investigations into resting-state connectivity using independent component analysis. Philos Trans R Soc Lond B Biol Sci 360:1001–1013.

Boorman L, Kennerley AJ, Johnston D, Jones M, Zheng Y, Redgrave P, Berwick J (2010): Negative blood oxygen level dependence in the rat: a model for investigating the role of suppression in neurovascular coupling. J Neurosci 30:4285–4294.

Bjørk M, Hagen K, Stovner L, Sand T (2011): Photic EEG-driving responses related to ictal phases and trigger sensitivity in migraine: A longitudinal, controlled study. Cephalalgia 31:444–455.

Bressler D, Spotswood N, Whitney D (2007): Negative BOLD fMRI response in the visual cortex carries precise stimulus-specific information. PLoS One 2:e410.

Brett M, Anton J, Valabregue R, Poline J (2002): Region of interest analysis using the MarsBar toolbox for SPM 99. Neuroimage 16:S497.

Buxton RB (2012): Dynamic models of BOLD contrast. Neuroimage 62:953–961.

Desikan RS, Ségonne F, Fischl B, Quinn BT, Dickerson BC, Blacker D, Buckner RL, Dale AM, Maguire RP, Hyman BT (2006): An automated labeling system for subdividing the human cerebral cortex on MRI scans into gyral based regions of interest. Neuroimage 31:968–980.

Devor A, Ulbert I, Dunn AK, Narayanan SN, Jones SR, Andermann ML, Boas DA, Dale AM (2005): Coupling of the cortical hemodynamic response to cortical and thalamic neuronal activity. Proc Natl Acad Sci USA 102:3822–3827.

Goense J, Merkle H, Logothetis NK (2012): High-resolution fMRI reveals laminar differences in neurovascular coupling between positive and negative BOLD responses. Neuron 76:629–639.

Grech R, Cassar T, Muscat J, Camilleri K, Fabri S, Zervakis M, Xanthopoulos P, Sakkalis V, Vanrumste B (2008): Review on solving the inverse problem in EEG source analysis. Journal of neuroengineering and rehabilitation 5:25.

Greicius MD, Krasnow B, Reiss AL, Menon V (2003): Functional connectivity in the resting brain: A network analysis of the default mode hypothesis. Proc Natl Acad Sci USA 100:253–258.

Hirota T, Yagyu T, Pascual-Marqui RD, Saito N, Kinoshita T (2001): Spatial structure of brain electric fields during intermittent photic stimulation. Neuropsychobiology 44:108–112.

Huber L, Goense J, Kennerley AJ, Ivanov D, Krieger SN, Lepsien J, Trampel R, Turner R, Möller HE (2014): Investigation of the

neurovascular coupling in positive and negative BOLD responses in human brain at 7T. Neuroimage 97:349–362.
Lansing RW, Thomas H (1964): The laterality of photic driving in normal adults. Electroencephalogr Clin Neurophysiol 16:290–294.
Laufs H, Kleinschmidt A, Beyerle A, Eger E, Salek-Haddadi A, Preibisch C, Krakow K (2003): EEG-correlated fMRI of human alpha activity. Neuroimage 19:1463–1476.
Lazarev VV, Pontes A, Mitrofanov AA (2015): Reduced interhemispheric connectivity in childhood autism detected by electroencephalographic photic driving coherence. J Autism Dev Disord 45:537–547.
Lee T, Girolami M, Sejnowski TJ (1999): Independent component analysis using an extended infomax algorithm for mixed subgaussian and supergaussian sources. Neural Comput 11:417–441.
Logothetis NK (2008): What we can do and what we cannot do with fMRI. Nature 453:869–878.
Logothetis NK, Wandell BA (2004): Interpreting the BOLD signal. Annu Rev Physiol 66:735–769.
Logothetis NK, Pauls J, Augath M, Trinath T, Oeltermann A (2001): Neurophysiological investigation of the basis of the fMRI signal. Nature 412:150–157.
Maggioni E, Molteni E, Arrigoni F, Zucca C, Reni G, Triulzi FM, Bianchi AM (2013): Coupling of fMRI and NIRS measurements in the study of negative BOLD response to intermittent photic stimulation. In: Engineering in Medicine and Biology Society (EMBC), 2013 35th Annual International Conference of the IEEE. Osaka: Japan, IEEE, pp 1378–1381.
Maggioni E, Arrubla J, Warbrick T, Dammers J, Bianchi AM, Reni G, Tosetti M, Neuner I, Shah NJ (2014): Removal of pulse artefact from EEG data recorded in MR environment at 3T. Setting of ICA parameters for marking artefactual components: Application to resting-state data. PloS one 9:e112147.
Maggioni E, Molteni E, Zucca C, Reni G, Cerutti S, Triulzi FM, Arrigoni F, Bianchi AM (2015): Investigation of negative BOLD responses in human brain through NIRS technique. A visual stimulation study. Neuroimage 108:410–422.
Moosmann M, Ritter P, Krastel I, Brink A, Thees S, Blankenburg F, Taskin B, Obrig H, Villringer A (2003): Correlates of alpha rhythm in functional magnetic resonance imaging and near infrared spectroscopy. Neuroimage 20:145–158.
Moosmann M, Eichele T, Nordby H, Hugdahl K, Calhoun VD (2008): Joint independent component analysis for simultaneous EEG–fMRI: Principle and simulation. Int J Psychophysiol 67: 212–221.
Müller NG, Kleinschmidt A (2004): The attentional'spotlight's' penumbra: Center-surround modulation in striate cortex. Neuroreport 15:977–980.
Mullinger K, Mayhew S, Bagshaw A, Bowtell R, Francis S (2014): Evidence that the negative BOLD response is neuronal in origin: A simultaneous EEG–BOLD–CBF study in humans. Neuroimage 94:263–274.
Murta T, Leite M, Carmichael DW, Figueiredo P, Lemieux L (2015): Electrophysiological correlates of the BOLD signal for EEG-informed fMRI. Hum Brain Mapp 36:391–414.
Neuner I, Warbrick T, Arrubla J, Felder J, Celik A, Reske M, Boers F, Shah NJ (2013): EEG acquisition in ultra-high static magnetic fields up to 9.4 T. Neuroimage 68:214–220.
Pascual-Marqui R, Esslen M, Kochi K, Lehmann D (2002): Functional imaging with low-resolution brain electromagnetic tomography (LORETA): A review. Methods Find Exp Clin Pharmacol 24:91–95.
Penny WD, Friston KJ, Ashburner JT, Kiebel SJ, Nichols TE. 2011. Statistical Parametric Mapping: The Analysis of Functional Brain Images: The Analysis of Functional Brain Images. Academic Press https://books.google.it/books?hl=it&lr=&id=G_qdEsDlkp0C&oi=fnd&pg=PP1ots=Xl1MFxU2XF&sig=dTm7w6qkO78qknZIl6ztuaYXsPM#v=onepage&q&f=false.
Sclocco R, Tana MG, Visani E, Gilioli I, Panzica F, Franceschetti S, Cerutti S, Bianchi AM (2014): EEG-informed fMRI analysis during a hand grip task: Estimating the relationship between EEG rhythms and the BOLD signal. Front Hum Neurosci 8:186.
Shmuel A, Yacoub E, Pfeuffer J, Van de Moortele P, Adriany G, Hu X, Ugurbil K (2002): Sustained negative BOLD, blood flow and oxygen consumption response and its coupling to the positive response in the human brain. Neuron 36:1195–1210.
Shmuel A, Augath M, Oeltermann A, Logothetis NK (2006): Negative functional MRI response correlates with decreases in neuronal activity in monkey visual area V1. Nat Neurosci 9:569–577.
Smith AT, Singh KD, Greenless MW (2000): Attentional Suppression of activity in the human visual cortex. Neuroreport 11: 271–278.
Smith AT, Williams AL, Singh KD (2004): Negative BOLD in the visual cortex: Evidence against blood stealing. Hum Brain Mapp 21:213–220.
Tana MG, Sclocco R, Bianchi AM (2012): GMAC: A Matlab toolbox for spectral Granger causality analysis of fMRI data. Comput Biol Med 42:943–956.
Tootell RB, Mendola JD, Hadjikhani NK, Liu AK, Dale AM (1998): The representation of the ipsilateral visual field in human cerebral cortex. Proc Natl Acad Sci USA 95:818–824.
van den Broek SP, Reinders F, Donderwinkel M, Peters M (1998): Volume conduction effects in EEG and MEG. Electroencephalogr Clin Neurophysiol 106:522–534.
van den Heuvel MP, Pol HEH (2010): Exploring the brain network: A review on resting-state fMRI functional connectivity. Eur Neuropsychopharmacol 20:519–534.
Visani E, Varotto G, Binelli S, Fratello L, Franceschetti S, Avanzini G, Panzica F (2010): Photosensitive epilepsy: Spectral and coherence analyses of EEG using 14Hz intermittent photic stimulation. Clin Neurophysiol 121:318–324.
Wade AR (2002): The negative BOLD signal unmasked. Neuron 36:993–995.